Acta Crystallographica Section A
Foundations of Crystallography
ISSN 0108-7673

Received 1 June 2010
Accepted 26 August 2010

Determination of Debye–Waller factor and structure factors for Si by quantitative convergent-beam electron diffraction using off-axis multi-beam orientations

X. H. Sang,* A. Kulovits and J. M. K. Wiezorek

Department of Materials Science and Mechanical Engineering, Swanson School of Engineering, University of Pittsburgh, 648 Benedum Hall, 3700 O'Hara Street, Pittsburgh, PA 15261, USA. Correspondence e-mail: xis20@pitt.edu

Debye–Waller (DW) factors and structure factors have been measured for Si using convergent-beam electron diffraction (CBED) experiments with a transmission electron microscope equipped with a field-emission gun and a post-column energy-filtering device. Si has been used here to evaluate the accuracy of multi-beam near-zone-axis orientations for the simultaneous refinement of DW factors and multiple structure factors. Strong dynamic interactions among different beams are obtained by tilting the crystal to specific four- or six-beam orientations near major zone axes, which provide sufficient sensitivity to determine accurate DW factors and structure factors. The DW factors of Si were measured using four-beam conditions near the [001] zone axis for temperatures ranging from 96 to 300 K. A comparison of the multi-beam near-zone-axis orientations with other CBED methods for DW and structure factor F_g refinement is presented.

1. Introduction

X-ray and electron diffraction experiments have been used successfully in the past to determine structure factors and also temperature factors, *i.e.* Debye–Waller (DW) factors (Zuo *et al.*, 1999; Jiang *et al.*, 2003; Tsuda & Tanaka, 1999; Ogata *et al.*, 2008). Based on sufficiently accurately measured sets of structure factors, the electron-density distribution in crystals can be determined experimentally, providing data of direct utility for validation of predictions from theory and computer simulations (Jiang *et al.*, 2003; Zuo *et al.*, 1999; Ogata *et al.*, 2008). Successful application of X-ray scattering techniques for structure-factor determination is limited to materials for which high-quality (low defect density) single crystals of sufficiently large dimensions (several hundred μm in linear dimensions) can be prepared. This typically has prevented experimental determination of electron-density distribution and bonding charge for metals and intermetallic systems using X-rays, since it is difficult to obtain crystals of sufficient size and quality. Using a contemporary transmission electron microscope (TEM), electron-beam probes as small as ∼0.2–1.0 nm in diameter can be formed routinely for the acquisition of convergent-beam electron diffraction (CBED) patterns. Hence, a major advantage of CBED methods with respect to X-ray methods is the reduced scale of the defect-free single-crystal sample volume that is required. For instance, using a 10 nm-diameter electron probe for a 100 nm-thick sample the CBED signal is generated from a material volume of about $\sim 8 \times 10^3\,\mathrm{nm}^3$ compared to the $\sim 3 \times 10^{16}\,\mathrm{nm}^3 = 3 \times 10^7\,\mu\mathrm{m}^3$ sample volume typically required for X-ray diffraction. As a result, quantitative CBED has been used for accurate measurement of structure factors and the experimental determination of electron density for a wide variety of materials, including some metals and intermetallics (Jiang *et al.*, 2003; Zuo *et al.*, 1999; Friis *et al.*, 2005).

Structure-factor measurements by quantitative CBED (QCBED) have utilized one of three different types of diffraction geometries, namely those associated with the so-called 'systematic row method' (Zuo *et al.*, 1999; Nüchter *et al.*, 1998), the zone-axis pattern (ZAP) method (Saunders *et al.*, 1999*a*,*b*) and the modified ZAP method (Tsuda & Tanaka, 1999). Each of these CBED methods has its advantages and disadvantages regarding electron-density determination from experimental measurements of accurate and precise structure factors.

The 'systematic row method' uses an incident-beam direction relative to the crystal that leads to one strongly excited diffracted beam or **g** vector, setting up a two-beam condition comprised of the strong transmitted and the singular diffracted beam. This leads to very strong interaction between the incident beam and the diffracted beam, and renders the intensities in the respective CBED discs very sensitive to changes in the corresponding structure factor F_g. Line profiles in the transmitted- and the diffracted-beam CBED discs are typically used for refinement (Zuo *et al.*, 1999; Nüchter *et al.*,

1998). This method requires the least computational time compared to the other two methods. However, it proves difficult to determine the exact incident-beam direction used in experiments and only one structure factor can be obtained from each CBED experiment.

For ZAP CBED (Saunders *et al.*, 1999*a*,*b*) the crystal is tilted into a high-symmetry or zone-axis orientation and the entire two-dimensional experimental CBED pattern is compared with a computer-calculated pattern. Unlike the systematic row method, where only two beams interact strongly with each other, in ZAP CBED several low-order diffracted beams, $\mathbf{g}_{hkl}$, interact dynamically, which allows for the simultaneous determination of multiple structure factors for beams in the zero-order Laue zone (ZOLZ). Additionally, the crystal orientation and the quality of the zone-axis pattern can be evaluated relatively easily by exploiting the symmetry of the ZAP. This method has been utilized rarely in the past, because of the significantly increased complexity of the refinement process and the associated increased computational effort relative to the line-profile-based refinements of the systematic row method. However, the increase in affordably available computing power over the past two decades has rekindled interest in the ZAP CBED method (Ogata *et al.*, 2008; Mueller *et al.*, 2009).

Tsuda & Tanaka (1999) modified the ZAP CBED method by including high-order Laue zone (HOLZ) beams in the refinement routine. Since the background for high-order discs is lower and more uniform than in ZOLZ discs it can be subtracted in HOLZ reflections with improved confidence. However, distortions caused by the electron optical lens system and the energy-filtering and imaging device (*e.g.* post-column Gatan imaging filter, GIF, or in-column Omega filter type and recording devices) of the TEM instrument increase with increasing scattering angle and therefore cannot be neglected in the HOLZ CBED discs. Correcting for such distortions has proved complicated and tends to introduce significant uncertainty to the refinement results, which at least partly negates the advantage regarding background subtraction offered by use of the HOLZ discs. The requirement for simultaneous acquisition of the ZOLZ and HOLZ discs in the modified ZAP CBED method implies the need to use a TEM instrument equipped with an in-column Omega-type energy-filtering device, since post-column energy-filtering devices currently restrict the scattering-angle range that can be acquired in single exposures to ZOLZ discs. Recently, Ogata *et al.* (2008) used modified ZAP CBED and near-zone-axis sample–beam orientations to determine DW factors and structure factors for Si simultaneously. They acquired CBED patterns of different sample–beam orientations, which were subsequently combined and refined simultaneously, allowing for robust and simultaneous refinement of DW factors and multiple structure factors.

Methods for CBED experiments that enable robust simultaneous refinements for DW factors and multiple structure factors are very desirable in the quest to determine experimentally electron densities in crystals. The room-temperature DW factors for atoms in the stable crystal structures of the elements, *e.g.* Si or Cu, are typically known from prior studies with sufficient accuracy for use as starting values in structure-factor refinements. However, the DW factors of the various atom species that constitute the unit-cell content for multi-elemental chemical compounds, *e.g.* metal oxide, nitride, carbide and boride phases and also for intermetallic compounds, are reasonably expected to vary from those known for the respective elements owing to the effects of interatomic bonding. For instance, the room-temperature DW factor for Al atoms in the face-centered-cubic (f.c.c.) structure of the element, $B(\mathrm{Al})_{\mathrm{f.c.c.}} = 0.86\ (1)\ \text{Å}^2$, is significantly different from that of Al atoms in the intermetallic compound NiAl with a chemically ordered primitive cubic structure of the CsCl type, $B(\mathrm{Al})_{\mathrm{NiAl}} = 0.47\ (1)\ \text{Å}^2$, as a result of the differences in interatomic bonding (Butt *et al.*, 1988; Georgopoulos & Cohen, 1977). Therefore, to determine experimentally the electron density and probe interatomic bonding in multi-elemental chemical compounds, it is necessary to refine DW factors and structure factors simultaneously. Ideally, this is accomplished by utilization of sufficiently information-rich data obtained from a single sample of the material in a single experimental TEM session, since this limits uncertainty arising from non-systematic effects, such as even minor variations in chemical composition between different samples of a given phase/material or significant changes in background intensities, for instance.

The current paper introduces different sample–beam orientations, which provide an effective combination of advantages of the systematic row method, *e.g.* reasonable computational effort, high-contrast dynamical features in the disc, and the ZAP method, *e.g.* easy determination of incident-beam direction, simultaneous determination of multiple structure factors, and are suitable for QCBED experimentation without the need for an in-column Omega-type energy-filtering-device-equipped TEM instrument. To achieve both high sensitivity for structure-factor and DW-factor refinement and easily examinable symmetry, CBED patterns are recorded for crystal orientations relative to the incident beam that are within a few Bragg angles of a low-order zone-axis orientation with three or more strongly diffracting beams. These orientations are referred to as multi-beam near-zone-axis orientations in the remainder of the paper. Dynamical interaction of four (transmitted and three diffracted beams) or six (transmitted and five diffracted) strongly excited beams restricts and distributes intensity uniformly among all excited discs, including the transmitted-beam or zero-beam disc. This constitutes a major advantage with regard to ZAP CBED in which the intensity in the center disc is always much higher compared to that of the diffracted-beam discs, corrupting intensities in the diffracted discs by background and noise. Additionally, it has been shown that off-zone-axis patterns are more sensitive to structure-factor changes than perfect on-axis ZAP (Burgess, 1994; Ogata *et al.*, 2008). Nakashima (2007) used off-zone-axis patterns to illustrate the advantage of improved background subtraction in quantification of CBED pattern intensities and successfully determined structure factors by QCBED without use of an energy filter. However,

the method was not applied specifically for DW factor determination.

To evaluate the accuracy of the multi-beam near-zone-axis orientations, zero-loss filtered CBED patterns have been acquired for single crystals of Si (space group $Fd\bar{3}m$, No. 227) using a post-column energy-filtering device attached to a field-emission-gun-equipped TEM instrument, and DW factors and structure factors have been measured at several temperatures ranging from 96 to 300 K, including those used in previous reports and adding one new temperature. Also, ZAP CBED experiments have been performed for Si. Results of the refinements for DW factors and structure factors obtained from the multi-beam near-zone-axis CBED method experiments for Si are compared with those from ZAP CBED experiments performed here and those reported in previous studies.

2. Experiments

2.1. Bloch wave calculation of CBED patterns

The interaction between fast electrons and crystals has been fully described (Bethe, 1928; Spence, 1993; Tsuda & Tanaka, 1995). In the Bloch wave formalism the electron wavefunction in a crystal with a periodical potential must satisfy the relativistically corrected Schrödinger equation as follows,

$$-\frac{h^2}{8\pi^2 m}\nabla^2\Psi(\mathbf{r}) - |e|V(\mathbf{r})\Psi(\mathbf{r}) = \frac{h^2K_o^2}{2m}\Psi(\mathbf{r}). \quad (1)$$

This equation can be solved by expanding the crystal potential and the wavefunction into Fourier series

$$V(\mathbf{r}) = \sum_g V_g \exp(2\pi i\mathbf{g}\cdot\mathbf{r}), \quad (2)$$

$$\Psi(\mathbf{r}) = \sum_g C_g(\mathbf{k})\exp[2\pi i(\mathbf{k}+\mathbf{g})\cdot\mathbf{r}]. \quad (3)$$

Substitution of equations (2) and (3) into equation (1) leads to a set of basis equations

$$[\mathbf{K}^2 - (\mathbf{k}+\mathbf{g})^2]^2 C_g(\mathbf{k}) + \sum_{h\neq g} U_h C_{g-h}(\mathbf{k}) = 0, \quad (4)$$

with $\mathbf{K}^2 = 2me(E+V_0)/h^2$ and $U_g = 2meV_g/h^2$. This eigenvalue problem can be solved using numerical methods. The jth eigenvalue $k^{(j)}$ and the jth eigenvector $C_g^{(j)}$ are calculated and form the jth branch of Bloch waves

$$\Psi^{(j)} = \sum_g C_g^{(j)} \exp\{2\pi i[\mathbf{k}^{(j)}+\mathbf{g}]\cdot\mathbf{r}\}. \quad (5)$$

Wavefunctions $\Psi(\mathbf{r})$ can then be expressed as a sum of Bloch waves with coefficients $c^{(j)}$, which are calculated using boundary conditions on the surfaces,

$$\Psi(\mathbf{r}) = \sum_j c^{(j)} \sum_g C_g^{(j)} \exp\{2\pi i[\mathbf{k}^{(j)}+\mathbf{g}]\cdot\mathbf{r}\}. \quad (6)$$

Rearranging terms in equation (6), the amplitude of reflection $\mathbf{g}$ at thickness t can be calculated:

$$\Phi_g(t) = \sum_j c^{(j)} C_g^{(j)} \exp[2\pi i k_z^{(j)} t], \quad (7)$$

provided that beam orientation, sample orientation, accelerating voltage and sample thickness are known. The intensity I along each $\mathbf{g}$ direction after dynamical interactions can be calculated based on equation (7) by

$$I = |\phi_g(t) * \phi_g(t)|. \quad (8)$$

We have used and adapted a public-domain simulation and refinement routine software, namely *MBFIT* (many-beam dynamical calculations and least-squares fitting), based on the Bloch wave formalism developed by Tsuda & Tanaka (1999). The initial values of the real parts of the electron-scattering structure factors are converted from X-ray structure factors, which are calculated based on atomic scattering factors from Doyle & Turner (1968). The imaginary part of the structure factors which takes into account thermal diffuse scattering (TDS) is calculated using a method described by Bird & King (1990).

2.2. Experimental CBED and data pre-processing

Experimental CBED patterns were acquired using a Jeol JEM 2100 F TEM operated at nominally 200 kV and equipped with a GIF TRIDIEM post-column energy filter (Gatan Inc.). A double-tilt cooling stage holder (Gatan Inc.) was used to acquire CBED patterns at temperatures as low as 96 K to reduce TDS. Zero-loss peak, energy-filtered CBED patterns were acquired using an electron-beam diameter of 0.5 nm, essentially eliminating the possible role of thickness variations on the CBED pattern intensity, with a 5–8 eV-wide energy-selecting slit and recorded on a charge-coupled device (CCD) camera with a maximum resolution of 2048 × 2048 and for sample temperatures of 96 K, 173 K and room temperature, 300 K.

The exact sample orientation with respect to the incident beam is important for the refinement process. In patterns obtained from thick regions, Kikuchi bands can be used to index the diffraction pattern and to determine crystal orientation with respect to the incident beam. In thinner sample regions, where Kikuchi bands are too weak or absent, features in the CBED discs are used for crystal orientation determination. In comparison to the ZAP method, the small crystal tilt away from the exact zone-axis orientation brings the respective diffracted-beam discs in the multi-beam near-zone-axis method we used very close to or exactly into Bragg conditions, *i.e.* the associated excitation error s_g is small or zero. This renders the contrast features resulting from dynamical beam interactions observed in the diffracted CBED discs to become coarser. The contrast feature periodicity in the discs is approximately proportional to the inverse of the effective excitation error $s_{\rm eff}$, which is given as

$$s_{\rm eff} = [s^2 + (1/\xi_g^2)]^{1/2} \quad (9)$$

with ξ_g the extinction distance. Then, the intensity, I, can be written as

$$I = \frac{1}{V}\left(\frac{\pi}{\xi_g}\right)^2 \frac{\sin^2(\pi s_{\rm eff}t)}{(\pi s_{\rm eff})^2}. \quad (10)$$

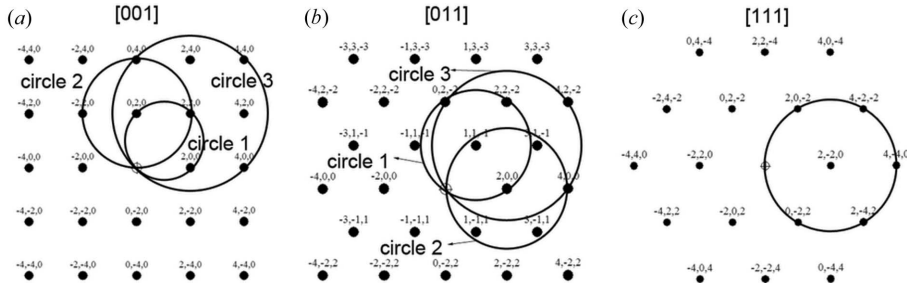

Figure 1
(*a*) Electron diffraction pattern of an f.c.c. structure along the [001] zone axis. Circles are traces of intersections between the Ewald sphere and the zero-order Laue plane. Two circles indicate beam directions in two four-beam conditions. (*b*) Electron diffraction pattern along [011]. (*c*) Electron diffraction pattern along [111].

A small s_g results in small $s_{\rm eff}$ and concomitantly in an enlarged or coarser periodicity in the contrast feature characteristic of the CBED disc. For data extraction from the experimentally acquired patterns coarser features prove to be less sensitive to small misalignment than finer features. Every point in each disc is associated with a beam direction and the intensity, $I_i^{\rm cal}$, is obtained using the Bloch wave method described above. Generally, a camera length is selected such that a disc contains more than 80 000 data points, which is sufficient to provide for accurate quantitative fitting and refinements.

2.3. Non-linear least-square fitting

Non-linear least-square fitting routines minimize the objective function S, which measures the difference between the observed experimental intensity, $I_i^{\rm obs}$, and the calculated intensity, $I_i^{\rm cal}$, and is defined as

$$S = \sum_i (I_i^{\rm obs} - cI_i^{\rm cal})^2, \qquad (11)$$

where c is a scale factor. By variation of parameters that are relaxed during the refinement, the computer program provides a minimum of S using a modified Marquardt method (Tsuda & Tanaka, 1995). Typically, the computer program can find a minimum in less than ten iterations. Assignment of different initial values for various parameters ascertains that the global minimum of S is found.

Some researchers prefer to include the background in the refinement process in order to relax the background (Saunders *et al.*, 1999*a*; Jiang *et al.*, 2003). We used an average value along a ring around each disc and assign this value as a constant background for the corresponding disc. That assumption has proven sufficient.

The goodness of fit (GOF) is evaluated using a weighted reliability factor (Tsuda & Tanaka, 1995)

$$R_{\rm w} = \left[\frac{\sum_i (I_i^{\rm obs} - cI_i^{\rm cal})^2/\sigma_i^2}{\sum_i (I_i^{\rm obs})^2/\sigma_i^2}\right]^2, \qquad (12)$$

with the standard deviation for the ith point, σ_i. Generally, it holds that $\sigma_i = (I_i^{\rm obs})^{1/2}$. The perfect fit between the observed and the calculated CBED patterns would result in an $R_{\rm w}$ value that is zero, *i.e.* when $I_i^{\rm obs}$ is identical to $cI_i^{\rm cal}$.

2.4. TEM sample preparation

The silicon sample used for TEM investigation was obtained from an Si single-crystal wafer with [001] surface normal and a thickness of 350 µm. Discs with a diameter of 3 mm were cut using a South Bay Technology Model 350 ultrasonic cutter. Those discs were then reduced in thickness to about 50 µm and mounted on copper rings. The final polishing to electron transparency was conducted using a Fischione Model 1010 low-angle ion milling and polishing system.

Prior to each TEM session the ion-milled Si TEM samples were plasma-cleaned using a South Bay Technology 'PC 2000' Plasma Cleaner to remove carbonaceous contamination from the sample surface.

3. Results: Debye–Waller factors and structure factors of silicon

Crystalline silicon is an f.c.c. structure that belongs to the space group ($Fd\bar{3}m$) (No. 227) with a motif of two symmetrically equivalent atoms situated at 0, 0, 0 and $\frac{1}{4}, \frac{1}{4}, \frac{1}{4}$. The lattice parameter used in this work is 0.543 nm. DW factors, structure factors and bonding properties of Si have been widely investigated by various methods, mainly because low-defect-concentration, single-crystalline silicon is relatively readily available and both X-ray and electron diffraction experiments yielded accurate results. Structure factors have been measured by Aldred & Hart (1973) using the X-ray *Pendellösung* method at liquid-nitrogen temperature and room temperature. Quantitative CBED measurements on Si have been attempted using the ZAP method (Saunders *et al.*, 1995) and the systematic row method (Ren *et al.*, 1997). DW factors were theoretically calculated by Reid & Pirie (1980) in a temperature range from 1 to 1000 K. Hence, Si is used in this study to evaluate the accuracy of our CBED method, as the results obtained can be readily compared with previously reported data.

3.1. Limited-beam diffraction conditions

Fig. 1 shows a number of different sample–beam orientations that constitute four- and six-beam near-zone-axis orientations. The circles in the reciprocal-space sections shown in Fig. 1 schematically represent intersections of the Ewald sphere with the ZOLZ. In each case, when the Laue center is close to the incident or zero beam (always in the center of the schematic reciprocal-space section depictions shown in Fig. 1), the contrast features in the CBED pattern result from strong interactions between low-order reflections among themselves and low-order reflections and the transmitted or zero beam, which makes the pattern very sensitive to the structure factors of excited reflections. For example, in the graphical representation of the diffraction geometries shown in Fig. 1(*a*), the

diffracted beams g_{200}, g_{220} and g_{020} are strongly excited simultaneously (circle 1), satisfying their respective Bragg conditions exactly. Therefore, the intensity distributions in the resulting CBED discs are sensitive to $F_g(200)$ and $F_g(220)$. In Fig. 1(*b*), using circle 1 g_{200}, g_{022} and g_{222} are in exact Bragg conditions, while g_{111} and g_{311} are near Bragg conditions, rendering these five low-order diffraction vectors strongly excited. This orientation enables the simultaneous determination of the structure factors of all five reflections from this one pattern. Circles 2 and 3 in Fig. 1(*a*, *b*) and the circle in Fig. 1(*c*) represent other examples of possible near-zone-axis multi-beam conditions. The interplay of the many beams in these near-zone-axis multi-beam orientations results in a sufficient number of equations that allow for simultaneous refinement of the DW factors and the structure factors. Conversely, in the systematic row method, only one diffracted beam is strongly excited, which results in an insufficient number of equations to determine simultaneously DW and structure factors robustly with high sensitivity.

Changing the crystal orientation such that the Laue center moves far away from the incident beam at the center of the reciprocal-space lattice section shown in Fig. 1, the intensity distributions in the resulting CBED discs become more sensitive to DW factors, as then only higher-order **g** reflections interact strongly with each other and are in exact Bragg conditions. The structure factors of high-order reflections can be approximated much better than low-order reflection structure factors by values based on free-atom data during the initial iterations of refinement of experimental data sets. Here, our approach is to use the four-beam conditions schematically described by circle 2 in Fig. 1(*a*) for the f.c.c. lattice to determine DW factors and to use the four-beam conditions illustrated by circle 1 in Fig. 1(*a*) to refine simultaneously multiple low-order structure factors. The current paper focuses on the DW factor determination aspect of the CBED experiments. In addition to the space-group absences, reflections with even indices obeying the condition $h + k + l = 4n + 2$ (n integer) also have zero intensity for spherical Si atoms. The four-beam diffraction condition used here for structure-factor refinement is therefore associated with excitation of $g_{\bar{2}20}$, g_{220} and g_{040} in Si (= condition I). Tilting the crystal even further away from the perfect [001] zone-axis orientation (Laue circle center coincident with the incident-beam direction), the four-beam condition for which g_{400}, g_{040} and g_{440} are excited is attained, which was used for the DW factor determination (= condition II; Fig. 1*a*, circle 3).

3.2. Experimental results

3.2.1. Si DW factor. We used the single-crystal Si to measure the accelerating voltage of the TEM instrument used for the CBED experiments following the HOLZ line matching technique (Zuo, 1992) and determined the voltage as 203 kV.

Near-[001] zone-axis CBED patterns in conditions I and II (Fig. 1) were recorded for Si at 96, 173 K and room temperature, 300 K. At each temperature CBED patterns were collected for a range of different sample thicknesses. The CBED patterns obtained for the diffracting condition II (Fig. 1) were used to determine DW factors of Si at these temperatures and a typical example pattern is shown in Fig. 2. Two-dimensional intensity data were extracted from the CBED discs for g_{000}, g_{040}, $g_{\bar{4}00}$ and $g_{\bar{4}40}$. Every pattern in condition II was refined using fixed structure factors based on free-atom values and relaxing the DW factor. The results for the CBED experiments performed at different temperatures and sample thicknesses are summarized in Fig. 3. Examples comparing the experimental and calculated CBED discs for the zero beam, 000, and the diffracted beams, 040, $\bar{4}00$ and $\bar{4}40$, used in the refinement for the DW factors are shown in Fig. 4. At the lower temperatures (96 and 173 K) the DW factors exhibit very small scatter (Fig. 3). With increasing sample thickness the signal-to-noise ratio in the CBED data increases, because the influence of residual surface contamination on the dynamical diffraction data decreases, which improves the accuracy of the refinements. The DW factors converge to an average value for each temperature as the thickness increases.

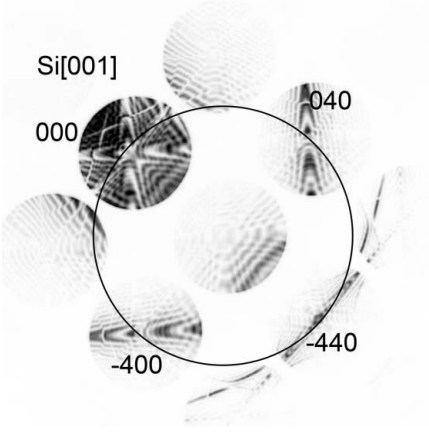

Figure 2
A condition-II Si CBED pattern obtained at 96 K. Refinement yielded a thickness of 343.5 nm. The black circle indicates the trace of the intersection of the Ewald sphere on the ZOLZ plane.

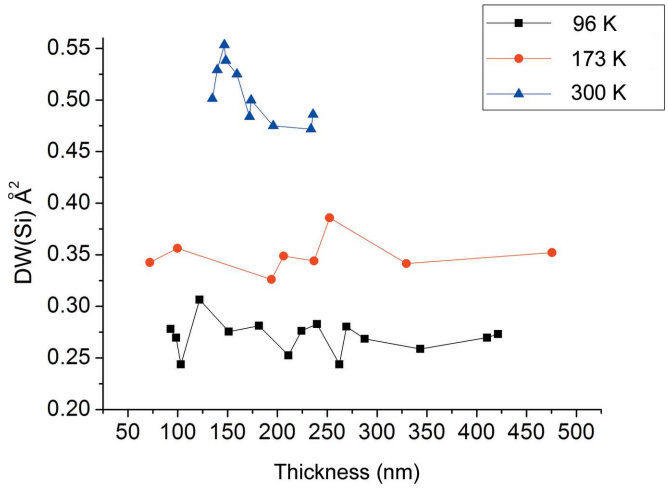

Figure 3
Refinement results for Si DW factors for different sample thickness at different temperatures.

Table 1
Comparison between experimental and theoretical Si DW factors.

Temperature (K)	Fitted Si DW factor and standard deviation (Å^2)	Theoretical DW factor (Å^2)			
		Reid & Pirie (1980)	Ogata *et al.* (2008)	Saunders *et al.* (1995)	Zuo *et al.* (1997)
96	0.2707 (162)	0.2446		0.26 (93 K)	
173	0.3476 (171)	0.3417			
300, t > 160 nm	0.4833 (110)	0.5275	0.463		0.4668

The refined DW factor values are systematically higher than the average for sample thicknesses less than 160 nm in the data obtained at room temperature. This can be attributed to surface contamination effects on the quality of the experimental CBED data. At room temperature the contamination rate is increased relative to the lower-temperature experimental conditions, increasing the uncertainty of DW factor measurements (Fig. 3) for sample thicknesses less than 160 nm. The scatter of the refined values for the DW factors at room temperature also tends to decrease as the thickness increases. At room temperature we could not acquire CBED patterns of sufficient quality for inclusion in the refinements from sample thicknesses in excess of 240 nm, because detrimental TDS contributions become intolerable for Si. Averaging our measurements for the different sample thicknesses yields the values and standard deviations for Si DW factors for the three different temperatures as summarized in Table 1. These values agree well with theoretical values and other experimental measurements for the measurements below room temperature. The discrepancy between the room-temperature DW factor reported by Ogata *et al.* and Zuo *et al.* and our data becomes negligible (less than 2%) after we reject the data obtained for sample thicknesses, t, below 160 nm, which may have been affected significantly by contamination during the CBED experimentation (Table 1).

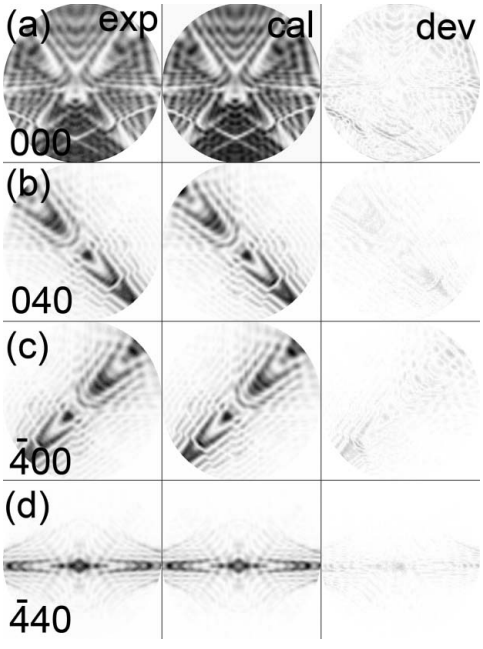

Figure 4
Comparison between simulated discs and experimental discs after refinement for the pattern shown in Fig. 2.

3.2.2. Si structure factors of the 220 and 400 reflections. For Si structure-factor refinement CBED patterns were acquired under condition I for different thicknesses at 96 and 173 K. An example of a typical CBED pattern taken under condition I is shown in Fig. 5. Pattern refinements were accomplished by relaxing $F_g(220)$ and $F_g(400)$ while using the DW factors determined experimentally here. We included 223 exact beams in the Bloch wave calculation without using the Bethe approximation. Si is a covalently bonded material and shows only relatively small charge transfer. Previous measurements (Aldred & Hart, 1973) have shown that the deviation of X-ray structure factors $F_g(220)$ from those obtained for the free-atom model due to covalent bonding is of the order of 1%. This small amount of change has minute influence on the intensity distribution in the CBED discs of the structurally allowed reflections. Hence, any method applied to determine structure or DW factors experimentally requires accuracies about an order of magnitude smaller than this small 1% change in the intensity due to the covalent bonding in Si. Fig. 6(*c*, *e*) illustrate that almost the entire profile can be approximated by the free-atom model (the gray line), except for the region enclosed in the black square, where the intensity predicted by the free-atom model is notably lower than the intensity observed experimentally. Fig. 6(*e*) clearly demonstrates that the four-beam method utilized here is highly sensitive to changes in F_g and suitable to detect the

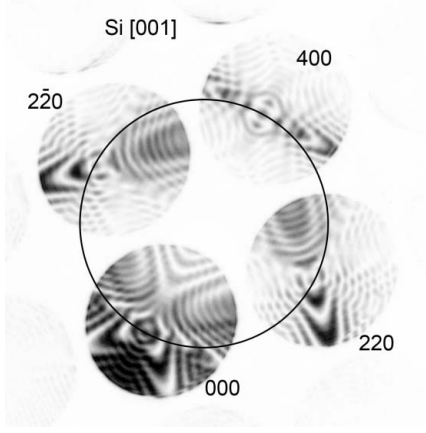

Figure 5
An Si CBED pattern acquired using condition I at 173 K. Refinement yielded a thickness of 371.6 nm. The black circle indicates the trace of the intersection of the Ewald sphere on the ZOLZ plane.

Table 2
Comparison between experimental and theoretical Si structure factors $F_g(220)$ and $F_g(400)$.

Structure factor	Present work at 96 K	Present work at 173 K	Aldred & Hart (1973)	Teworte & Bonse (1984)†	Ogata *et al.* (2008)‡	Free atom
$F_g(220)$	8.659 (8)	8.654 (8)	8.651	8.682	8.685	8.712
$F_g(400)$	7.456 (13)	7.440 (28)	7.444	7.446	7.478	7.511

† DW factor is set to be 0.4 Å^2 to convert it to X-ray scattering factor per Si atom. ‡ DW factor is set to be 0.463 Å^2 to convert it to X-ray scattering factor per Si atom.

smallest differences between the true F_g of the structure and approximated F_g values. The refined values of $F_g(220)$ and $F_g(400)$ are plotted *versus* sample thickness at 96 and 173 K in Fig. 7. We converted the electron structure factors to X-ray structure factors using the Mott formula. As the thickness increases the structure factors tend to converge. A similar trend was observed during DW factor refinement and residual surface contamination is a possible cause of it. The standard deviation for structure factors during each refinement is small compared to deviations observed in separate refinement attempts. Hence, we report here the statistical errors in terms of the equivalent of one standard deviation. The average values and errors corresponding to one standard deviation, which is $s = [(1/N-1)\sum_{i=1}^{N}(x_i-\overline{x})^2]^{1/2}$, are calculated and for $F_g(220)$ and $F_g(400)$ listed in Table 2 together with values from prior reports. The results reported here are consistent with previously reported values.

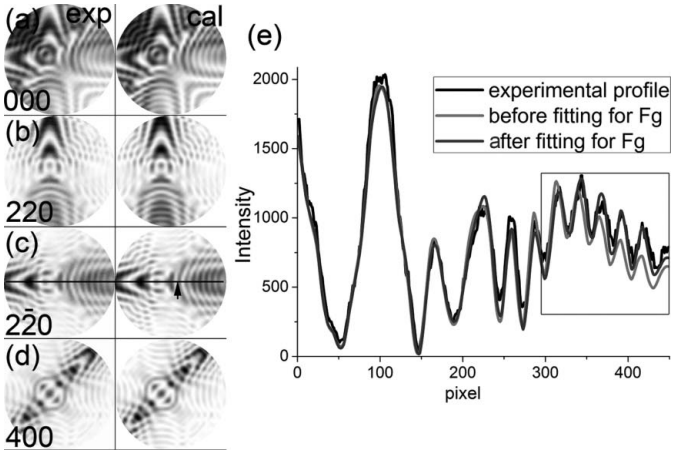

Figure 6
(*a*) to (*d*) Comparison between simulated discs and experimental discs after fitting for the pattern shown in Fig. 5. R_w = 0.136 after refinement. (*e*) Intensity profiles along the black line trace in (*c*) pointed to by an arrow for the experimental disc, the simulated disc based on free-atom data and the simulated disc after structure-factor refinement.

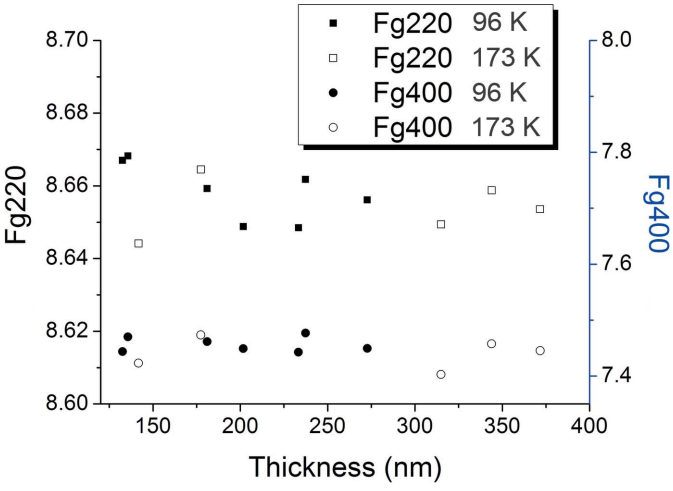

Figure 7
Refinement results of silicon structure factors $F_g(220)$ and $F_g(400)$ from different sample thicknesses at different temperatures.

4. Discussion

4.1. Multi-beam near-zone-axis method

4.1.1. Intensity sensitivity with changes in structure factor F_g. The systematic row CBED pattern method has been known as sufficiently sensitive for refinement of the structure factor F_g of the excited beam in the two-beam condition. Accurate Bloch wave solutions have been determined (Spence & Zuo, 1992). When the excitation error s_g is zero, the intensity of the transmitted beam, I_0, can be written as (Spence & Zuo, 1992)

$$I_0 = \cos^2\left(\frac{\pi t|U_g|}{K_n}\right), \tag{13}$$

with K_n the wavevector component in the beam direction, U_g the structure factor of the excited beam **g**, and t is the thickness. The partial derivative of I_0 with respect to the structure factor U_g is given as

$$\frac{\partial I_0}{\partial U_g} = -\frac{\pi t}{K_n}\sin\left(\frac{2\pi t|U_g|}{K_n}\right). \tag{14}$$

For a four-beam condition with a sample–beam orientation such that the Ewald sphere intersects the ZOLZ at circle 1 in Fig. 1(*a*), g_1, g_2 and g_3 are excited. g_1 and g_2 have the same structure factor U_g, and the structure factor of g_3 is U_m. When s_{g_1}, s_{g_2} and s_{g_3} are all zero, the exact solution of the intensity of the transmitted beam can be written as (Fukuhara, 1966)

$$I_0 = \frac{3}{8} + \frac{1}{8}\cos\left(\frac{4\pi t|U_g|}{K_n}\right) + \frac{1}{2}\cos\left(\frac{2\pi t|U_m - U_g|}{K_n}\right). \tag{15}$$

From equation (15) follows the derivative of I_0 with respect to structure factor U_g,

$$\frac{\partial I_0}{\partial U_g} = -\frac{2\pi t}{K_n}\sin\left(\frac{4\pi t|U_g|}{K_n}\right) + \frac{\pi t}{K_n}\sin\left(\frac{2\pi t|U_m - U_g|}{K_n}\right). \tag{16}$$

Table 3
Comparison of R_w for Si structure-factor refinement with the ZAP CBED method and the multi-beam near-zone-axis CBED method according to condition I (Fig. 1).

Si	Thickness (Å)	R_w using free-atom model	R_w $F_g(220)$ is relaxed	R_w $F_g(220)$ and $F_g(400)$ are relaxed
Room temperature, zone-axis pattern	1437.10	0.241	0.235	0.231
	2228.98	0.217	0.210	0.209
	2725.49	0.289	0.283	0.281
Room temperature, condition I	2001.58	0.181	0.170	0.169
	1718.33	0.187	0.181	0.179
	1407.29	0.184	0.178	0.177
Liquid-nitrogen temperature, condition I	1324.98	0.152	0.147	0.145
	1354.87	0.139	0.131	0.129
	1809.41	0.135	0.122	0.119

$\partial I_0/\partial U_g$ has been plotted for different thicknesses for both the two-beam condition and the multi-beam orientation of condition I for Si (Fig. 8). U_g is set to be 0.04 Å^{-2} and U_m is 0.024 Å^{-2}. K_n is calculated using an accelerating voltage of 200 kV. Fig. 8 shows that generally the intensity for the four-beam condition is more sensitive to changes in structure factor than for the two-beam condition. It is also discernible that with increasing thickness the magnitude of $\partial I_0/\partial U_g$ increases. CBED patterns from thick areas are more sensitive to structure factors. However, CBED patterns from thick areas are also always noisy and exhibit diminished contrast, because of high absorption and also potential defect content in the scattering volume of the material. As there are no analytical solutions for the ZAP method (Fukuhara, 1966) it could not be included in this part of the discussion. While the ZAP method might also be very sensitive to changes in structure factor, the treatment of the background and the differences in intensity distribution in the center disc compared to the diffracted discs at higher scattering angle compromise the precision and accuracy that can be attained in the ZAP method, which is reflected in the typically large R_w values that are obtained (Table 3).

4.1.2. R_w value. The R_w value is used here to evaluate the goodness of the fit. Smaller R_w values correspond to increased reliability and reduced uncertainty of the refinement result. We have performed ZAP CBED experiments for comparison with the multi-beam near-zone-axis CBED method in order to provide a direct comparison regarding the goodness of fit and robustness of the refinements of structure factors. The results of this comparison are summarized in Table 3. Table 3 shows that R_w is in general significantly higher for ZAP CBED compared to the four-beam condition. In ZAP CBED, the intensity of the transmitted beam is orders of magnitude larger than for the diffracted beams, unless the pattern is recorded in a very thick region. Hence, ZAP CBED data sets are subjected to noise and Kikuchi bands, which makes the background subtraction difficult. Even though the intensity distributions in discs affected by Kikuchi bands and noise are corrupted, those discs still have to be included in the refinement as the intensity distribution in the center disc alone does not provide sufficient information for robust refinements of the structure factors and DW factors. Conversely, in the multi-beam (four-beam or six-beam) conditions, the intensity is evenly distributed between the transmitted and the respective diffracted beams. Every disc contains sufficient intensity to reduce the usually detrimental influence of noise and inelastic scattering. Therefore the magnitudes of R_w can be significantly reduced if CBED patterns are obtained in these types of multi-beam near-zone-axis orientations. Cooling the sample to liquid-nitrogen temperature results in further improvement of the goodness of fit, *i.e.* a reduction of the R_w (Table 3).

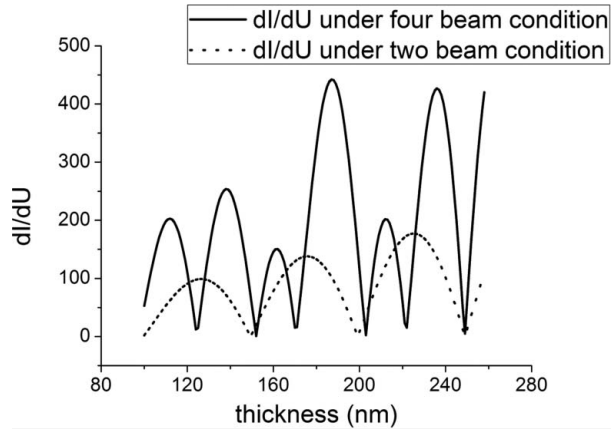

Figure 8
Plot of $\partial I_0/\partial U_g$ at different beam conditions for different thicknesses.

4.1.3. Beam selection. Although multi-beam near-zone-axis CBED pattern orientations are more sensitive than zone-axis pattern or two-beam conditions regarding structure-factor changes, it was found in this work that it can be disadvantageous to include all diffracted beams in the refinement. Generally in the ZAP as well as the multi-beam near-zone-axis method not every disc is sensitive to structure-factor changes. The inclusion of structure-factor-insensitive discs in the calculation can introduce large errors, rendering the refinement useless. While it can prove rather difficult in the ZAP method to find criteria to determine which beams to include and which to discard, the selection criterion for the multi-beam near-zone-axis method is relatively straightforward. Strongly diffracting beams with $s = 0$ interact strongly with each other and the transmitted beam, and are very sensitive to changes in structure factor. Diffracted beams with large excitation errors s that interact only very weakly with all the other beams can be quite insensitive to structure-factor changes. Inclusion of diffracted beams with large s can

increase R_w from 0.15 to 0.4. Hence, only discs that fulfill the Bragg condition should be included in the refinement.

4.2. DW and structure factor determination of crystalline Si

The multi-beam near-zone-axis method has been successfully applied to determine low-order structure factors and DW factors for Si at three different temperatures. Table 1 shows very good agreement between the measured DW factors and theoretically estimated values at the three different temperatures (Reid & Pirie, 1980). The experimentally determined DW factors have subsequently been used to refine the structure factors for the 220 and 400 reflections. Table 2 shows that structure factors obtained at different temperatures are consistent and in good agreement with literature results (Aldred & Hart, 1973; Teworte & Bonse, 1984; Ogata *et al.*, 2008). These experimentally obtained results for crystalline Si demonstrate that the multi-beam near-zone-axis CBED method has successfully been applied to obtain quantitative values for structure and DW factors. This result shows that the multi-beam near-zone-axis CBED method is accurate and sensitive enough to allow structure and Debye–Waller factor refinement with less than 1% error, which is a requirement for electronic structure determination to probe the effects of bonding. Hence, the results obtained by this method are suitable for experimental electronic structure determination.

5. Conclusion

We have described the application of a multi-beam near-zone-axis CBED method, a modified zone-axis CBED method, to improve the accuracy of determination of DW factors and multiple structure factors. By selecting four-beam conditions near the [001] zone axis, we successfully determined DW factors at three different temperatures [B(Si) = 0.2707 Å^2 at 96 K, B(Si) = 0.3476 Å^2 at 173 K and B(Si) = 0.5063 Å^2 at 300 K] and the F_g(220) (8.659 at 96 K and 8.654 at 173 K) and F_g(400) (7.456 at 96 K and 7.440 at 173 K) structure factors with very high accuracy. We thereby successfully verified the validity of the method.

This work was supported by a grant from the Office of Basic Energy Sciences, a division of Materials Science and Engineering, of the US DOE (grant No. DE-FG02-08ER46545).

References

Aldred, P. J. E. & Hart, M. (1973). *Proc. R. Soc. London A Mater.* **332**, 223–238.
Bethe, H. (1928). *Ann. Phys. Berlin*, **392**, 55–129.
Bird, D. M. & King, Q. A. (1990). *Acta Cryst.* A**46**, 202–208.
Burgess, W. G. (1994). PhD thesis, Cambridge University, England.
Butt, N. M., Bashir, J., Willis, B. T. M. & Heger, G. (1988). *Acta Cryst.* A**44**, 396–399.
Doyle, P. A. & Turner, P. S. (1968). *Acta Cryst.* A**24**, 390–397.
Friis, J., Jiang, B., Marthinsen, K. & Holmestad, R. (2005). *Acta Cryst.* A**61**, 223–230.
Fukuhara, A. (1966). *J. Phys. Soc. Jpn*, **21**, 2645–2662.
Georgopoulos, P. & Cohen, J. B. (1977). *Scr. Metall.* **11**, 147–150.
Jiang, B., Zuo, J. M., Jiang, N., O'Keeffe, M. & Spence, J. C. H. (2003). *Acta Cryst.* A**59**, 341–350.
Mueller, K., Schowalter, M., Jansen, J., Tsuda, K., Titantah, J., Lamoen, D. & Rosenauer, A. (2009). *Ultramicroscopy*, **109**, 802–814.
Nakashima, P. N. H. (2007). *Phys. Rev. Lett.* **99**, 125506.
Nüchter, W., Weickenmeier, A. L. & Mayer, J. (1998). *Acta Cryst.* A**54**, 147–157.
Ogata, Y., Tsuda, K. & Tanaka, M. (2008). *Acta Cryst.* A**64**, 587–597.
Reid, J. S. & Pirie, J. D. (1980). *Acta Cryst.* A**36**, 957–965.
Ren, G., Zuo, J. M. & Peng, L. M. (1997). *Micron*, **28**, 459–467.
Saunders, M., Bird, D. M., Zaluzec, N. J., Burgess, W. G., Preston, A. R. & Humphreys, C. J. (1995). *Ultramicroscopy*, **60**, 311–323.
Saunders, M., Fox, A. G. & Midgley, P. A. (1999*a*). *Acta Cryst.* A**55**, 471–479.
Saunders, M., Fox, A. G. & Midgley, P. A. (1999*b*). *Acta Cryst.* A**55**, 480–488.
Spence, J. C. H. (1993). *Acta Cryst.* A**49**, 231–260.
Spence, J. C. H. & Zuo, J. M. (1992). *Electron Microdiffraction.* New York: Plenum Press.
Teworte, R. & Bonse, U. (1984). *Phys. Rev. B*, **29**, 2102–2108.
Tsuda, K. & Tanaka, M. (1995). *Acta Cryst.* A**51**, 7–19.
Tsuda, K. & Tanaka, M. (1999). *Acta Cryst.* A**55**, 939–954.
Zuo, J. M. (1992). *Ultramicroscopy*, **41**, 211–223.
Zuo, J. M., Blaha, P. & Schwarz, K. (1997). *J. Phys. Condens. Matter*, **9**, 7541–7561.
Zuo, J. M., Kim, M., O'Keeffe, M. & Spence, J. C. H. (1999). *Nature* (*London*), **401**, 49–52.